MATERIALS SCIENCE

Potential energy–driven spin manipulation via a controllable hydrogen ligand

Peter Jacobson,[1]*†‡ Matthias Muenks,[1‡] Gennadii Laskin,[1] Oleg Brovko,[2] Valeri Stepanyuk,[3] Markus Ternes,[1]* Klaus Kern[1,4]

Spin-bearing molecules can be stabilized on surfaces and in junctions with desirable properties, such as a net spin that can be adjusted by external stimuli. Using scanning probes, initial and final spin states can be deduced from topographic or spectroscopic data, but how the system transitions between these states is largely unknown. We address this question by manipulating the total spin of magnetic cobalt hydride complexes on a corrugated boron nitride surface with a hydrogen-functionalized scanning probe tip by simultaneously tracking force and conductance. When the additional hydrogen ligand is brought close to the cobalt monohydride, switching between a correlated $S = {}^1/_2$ Kondo state, where host electrons screen the magnetic moment, and an $S = 1$ state with magnetocrystalline anisotropy is observed. We show that the total spin changes when the system is transferred onto a new potential energy surface that is defined by the position of the hydrogen in the junction. These results show how and why chemically functionalized tips are an effective tool to manipulate adatoms and molecules and a promising new method to selectively tune spin systems.

INTRODUCTION

The magnetic behavior of adatoms and single molecular magnets on surfaces is usually defined by static parameters, such as local symmetry, spin-orbit interaction, or exchange coupling with the electron bath of the host (*1*–*5*). However, there is a widespread interest in actively controlling molecular and adatom spin states for switching applications (*6*, *7*). Beyond imaging and spectroscopy, scanning probes are atomically precise manipulation tools (*8*, *9*). When manipulation and spectroscopy operate in tandem, it is possible to observe the formation of chemical bonds and continuously tune the exchange interaction between magnetic impurities (*10*–*13*). Tip functionalization, now routinely used to create chemically precise contacts where a molecule acts as a transducer, is one promising method to control spins (*14*–*18*). This strategy has its roots in small-molecule adsorption on metal-bearing porphyrins and phthalocyanines (*19*, *20*) and capitalizes on two strengths of local probes: the ability to address specific atomic sites and the variable width of the tunnel junction. With magnetic adatoms gaining prominence as model quantum systems, it is highly desirable to understand how chemically reactive probes couple to and influence the measurement process and eventually control the resulting magnetic state.

Here, we reversibly control the total spin of cobalt hydride (CoH) spin centers adsorbed on the *h*-BN/Rh(111) moiré by manipulating a single hydrogen atom with the tip of a combined scanning tunneling microscope (STM) and a noncontact atomic force microscope (AFM). As the distance z between the probing tip and the CoH complex decreases, hydrogen initially adsorbed on the tip apex weakly bonds to the CoH complex, inducing rapid transitions between a correlated $S = {}^1/_2$ Kondo state and an anisotropic $S = 1$ state. Local spectroscopy identifies a stable total spin at high and low values of the conductance, whereas at intermediate conductance, dynamic switching is observed. By combining conductance-distance [$G(z)$] and force-distance [$F(z)$] measurements together with density functional theory (DFT) calculations, we unravel the microscopic potential energy landscapes present within the tunnel junction. We demonstrate that, by coupling a functionalized tip to an undercoordinated adatom, the reactivity of the adatom can be harnessed to drive transitions between different total spin states. The spin within the tunnel junction can therefore be actively monitored and reversibly controlled with single-atom precision.

RESULTS

Figure 1A shows a constant current image of CoH complexes on *h*-BN/Rh(111). The lattice mismatch between the Rh(111) substrate and the single monolayer of *h*-BN results in a strongly corrugated surface with 3.2-nm periodicity, on which the CoH complexes appear as bright protrusions. A clear indication of hydrogen adsorption on the tip apex is the sharp change in tip height, reduced by 20 pm (Fig. 1A, red dashes), while imaging the *h*-BN/Rh(111) surface in constant current mode (*21*). Figure 1B shows constant current images of an individual CoH complex located near the rim-valley boundary of *h*-BN/Rh(111) that is imaged with a hydrogen-functionalized tip. At low junction conductance ($G = I_S/V_S = 1.61 \times 10^{-4}\ G_0$; $G_0 = 77.48\ \mu S$; the quantum of conductance), corresponding to relatively large tip-sample separations z, the increased contrast due to the hydrogen in the junction partially overlaps a CoH complex (Fig. 1B, bottom panel). As G is increased, this boundary region transitions to a noise-speckled circle with a brighter appearance, that is, larger z height, to compensate for an overall increase in the conductance. Given the strong G dependence within this narrow range, these results hint that the observed contrast is not solely due to the local topography but is also due to mechanical and electronic changes in the junction. These images are qualitatively similar to measurements of undercoordinated metal adatoms in the presence of adsorbed hydrogen (*22*, *23*). Because the hydrogen content of the CoH_x complex governs the spin state (*5*), dI/dV spectroscopy was performed while varying the setpoint conductance G with the tip positioned over the central region. At the lowest conductance, $G = 6.45 \times 10^{-4}\ G_0$ (Fig. 1C, bottom curve), the spectra show two symmetric steps around zero bias with increasing differential conductance. These steps originate from the inelastic spin

[1]Max Planck Institute for Solid State Research, Heisenbergstrasse 1, 70569 Stuttgart, Germany. [2]Abdus Salam International Centre for Theoretical Physics, Trieste, Italy. [3]Max Planck Institute of Microstructure Physics, Weinberg 2, 06120, Halle (Saale), Germany. [4]Institut de Physique, École Polytechnique Fédérale de Lausanne, CH-1015 Lausanne, Switzerland.
*Corresponding author. Email: peter.jacobson@uni-graz.at (P.J.); m.ternes@fkf.mpg.de (M.T.)
†Present address: Institute of Chemistry, University of Graz, 8010 Graz, Austria.
‡These authors contributed equally to this work.

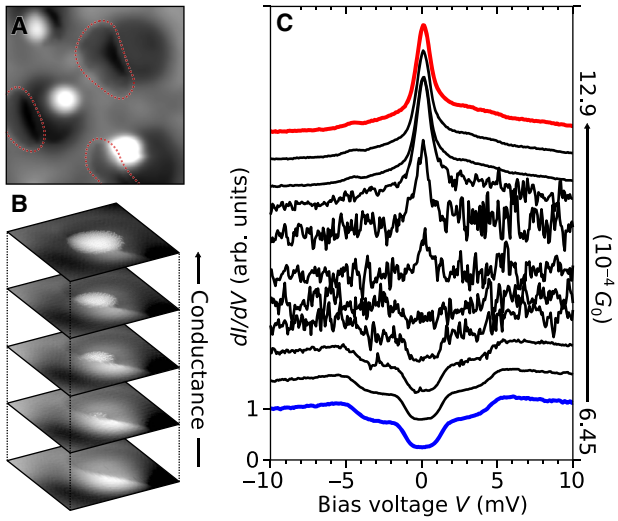

Fig. 1. Influence of hydrogen-functionalized tips on imaging and spectroscopy. (**A**) Constant current STM image (approximately 5 × 5 nm^2; V = −15 mV, I = 20 pA, G = 1.72 × 10^{-5} G_0) of CoH complexes on the *h*-BN/Rh(111) moiré obtained with a hydrogen-functionalized tip. Areas with enhanced contrast due to hydrogen in the junction are circled in red. (**B**) Constant current STM images (1.2 × 1.2 nm^2; top to bottom: V = −0.3, −0.7, −1.0, −1.3, and −1.6 mV; I = 20 pA, corresponding to G = 8.60 × 10^{-4}, 3.69 × 10^{-4}, 2.58 × 10^{-4}, 1.99 × 10^{-4}, and 1.61 × 10^{-4} G_0) of a CoH complex highlighting the strong conductance (tip-sample distance) dependence of imaging with a hydrogen-functionalized tip. (**C**) Local spectroscopy obtained on the CoH complex in (B). The tip was centered on the bright lobe (G = 1.61 × 10^{-4} G_0). At G = 6.45 × 10^{-4} G_0 (blue), a set of double steps is observed, indicative of a spin 1 complex with magnetic anisotropy. Increasing the conductance in steps of ΔG = 0.16 × 10^{-4} G_0 leads to unstable spectra until a spin $^1/_2$ Kondo peak emerges at high conductance (red; G = 12.9 × 10^{-4} G_0). All spectra are normalized to the differential conductance at −10 mV; normalized spectra are offset by 0.5. arb. units, arbitrary units.

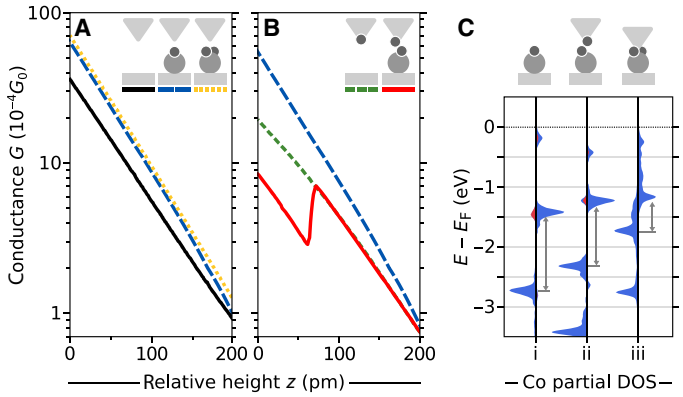

Fig. 2. Conductance-distance spectroscopy. (**A**) Conductance-distance, $G(z)$, curves obtained with a bare Pt tip on *h*-BN (black), CoH (dashed blue), and CoH_2 (dotted yellow) at a tip-sample bias of V = −10 mV. (**B**) Using a functionalized tip, CoH + H_{tip} (red), a conductance discontinuity, corresponding to the S = 1 to S = $^1/_2$ total spin change, is observed at a relative height z of 70 pm. The functionalized tip approaching the substrate, *h*-BN + H_{tip} (dashed green), shows no discontinuity and has a nonexponential character. For direct comparison, the CoH $G(z)$ measurement from (A) is plotted again (dashed blue). Inverse decay constants, κ_G: (A) *h*-BN (black), 8.7 ± 0.1 nm^{-1}; CoH (dashed blue), 9.9 ± 0.1 nm^{-1}; CoH_2 (dotted yellow), 9.8 ± 0.1 nm^{-1}; (B) *h*-BN + H_{tip} (dashed green), 6.6 ± 0.3 nm^{-1} (0 < z < 70 pm) and 7.7 ± 0.4 nm^{-1} (70 pm < z < 200 pm); CoH + H_{tip} (red), 6.9 ± 0.4 nm^{-1} (0 < z < 70 pm) and 8.5 ± 0.5 nm^{-1} (70 pm < z < 200 pm). The color-coded insets schematically depict the junction geometry. (**C**) Plots of majority (left) and minority (right) spin-projected density of states (blue, *d* orbitals; red, *sp* orbitals) of an S = 1 CoH complex. The first plot shows a magnetic moment of 2.0 μ_B (without tip) (i), the second plot shows a slight magnetic moment reduction (1.6 μ_B) due to the presence of a hydrogen-functionalized tip (ii), and the third plot shows the transition from S = 1 to S = $^1/_2$ (1.2 μ_B) at close tip distances (iii). The change in Stoner splitting between majority and minority bands is schematically depicted with vertical gray arrows.

excitations of a CoH complex with a total spin S = 1, where magnetocrystalline anisotropy has removed the 3d-level degeneracy. Increasing G by decreasing the tip-sample separation z results in progressively unstable spectra until the emergence of a stable zero bias peak at G = 12.9 × 10^{-4} G_0, identified as an S = $^1/_2$ CoH_2 Kondo resonance (*5*). This transition is fully reversible, and the initial S = 1 total spin state is restored when the junction conductance is reduced (see fig. S1). We observe a metastable state, when G is between 8 × 10^{-4} G_0 and 11 × 10^{-4} G_0, where the hydride complex randomly transitions between the S = 1 and S = $^1/_2$ states on a time scale of 100 ms. The change in tip-sample separation for this conductance range corresponds to a Δz of less than 25 pm. Note that this metastable behavior does not depend on the bias voltage during the spectroscopic measurement (see also fig. S2). Differential conductance (dI/dV) spectroscopy not only identifies the spin state but also aids in the interpretation of the STM images in Fig. 1B. The constant current images in Fig. 1B were obtained over a bias range (0.3 to 1.6 mV) where the topographic appearance is closely linked to the features in the dI/dV measurements and, therefore, at small bias voltages, is dominated by the Kondo resonance.

To investigate the switching behavior in detail, we performed $G(z)$ measurements over CoH_x complexes and bare *h*-BN. Approaching *h*-BN as well as CoH_x complexes with a bare tip reveals a strictly exponential increase in conductance, $G(z) = G_0\exp(-2\kappa_G(z_0 + z))$, where κ_G is the decay rate and z_0 is the tip height at the initial setpoint conductance G (Fig. 2A). Functionalizing the tip apex with hydrogen alters the junction conductance characteristics, with $G(z)$ showing a less than exponential increase and a reduced κ_G compared to the data obtained with a bare tip (Fig. 2B). This characteristic behavior is similar to the observations of Weiss *et al.* (*18*) on a complex organic molecule with a hydrogen-functionalized tip. However, when approaching a CoH complex with a hydrogen-functionalized tip, $G(z)$ closely follows the *h*-BN trace until the conductance rapidly decreases by a factor of 2.5, indicating the S = 1 to S = $^1/_2$ transition (Fig. 2B, red) that is observed by local spectroscopy in Fig. 1C. Therefore, the drop in conductance stems from both the direct transfer of hydrogen within the junction, altering the geometry and modifying the tunnel barrier, and the relative change in total conductance between the CoH and CoH_2 complexes.

To understand the electronic structure modification in the spin-switching process, we performed DFT calculations for various representative junction geometries (Fig. 2C). A CoH complex on *h*-BN exhibits a nearly free atom–like electronic structure (Fig. 2C, i), with Stoner split 3d levels giving it a magnetic moment of 2.0 μ_B (Bohr magneton) (*5*). Approaching the complex with a Pt tip, which has a hydrogen atom bound to its apex (Fig. 2C, ii), gradually introduces indirect bonding via the H of the CoH complex, resulting in the reduction of the Co magnetic moment (Fig. 2C, ii). The magnetic moment of Co remains close to 2 μ_B, an effective S = 1 state, until the approaching functionalized tip brings the H *sp* orbitals into direct overlap with the Co *d* orbitals (Fig. 2C, iii). Bonding of two H atoms to Co, as shown in our previous work, is strong enough to partially quench the magnetic moment of Co, reducing it to 1.2 μ_B, an effective S = $^1/_2$ state.

To reveal the microscopic forces at work in the spin transition, we track the frequency shift, Δf, of the oscillating tuning fork from its non-interacting resonance frequency, f_0 = 29,077 Hz. We measure $\Delta f(z)$ curves

over switching complexes and the bare *h*-BN. To remove the long-range forces between the extended tip and the sample, we subtract the background from the data, that is, $\Delta f = \Delta f_{\mathrm{CoH}} - \Delta f_{h\text{-BN}}$ (see Materials and Methods and fig. S3). The Δf is small and negative before rapidly decreasing upon approach (Fig. 3A, black). This sharp drop in Δf coincides with a change in the $G(z)$ measurement similar to that in Fig. 2B; however, here, this feature is broadened because of averaging over the 100-pm oscillation amplitude (Fig. 3A, gray). Short-range forces, $F(z')$, were quantified by converting $\Delta f(z)$ using the method of Sader and Jarvis (*24*). Before the $S = 1$ to $S = {}^1/_2$ transition, the force between the tip and sample is weakly attractive and grows exponentially upon approach. As the hydrogen on the tip apex couples to the CoH complex, the attractive force grows steeply over a transition region of 35 pm before leveling off (Fig. 3B). The instantaneous junction conductance, $G(z')$, is deconvoluted to remove the influence of an oscillating tip (*25*), revealing that the force and conductance transition regions coincide.

From the $F(z')$ measurement, we reconstruct the one-dimensional (1D) potential energy landscape, $U(z')$, across the spin transition by integrating $F(z')$ (Fig. 3C). The $U(z')$ curve shows a steep change in slope as the tip brings the hydrogen closer to the CoH complex, suggestive of a transition between potential energy surfaces. This interpretation is broadly in line with a framework recently developed by Hapala *et al.* (*26*) to describe high-resolution AFM imaging with functionalized tips. One key component of this model is that the probe particle, hydrogen in our case, not only follows the lowest potential energy surface but also undergoes relaxation within the junction. In our $U(z')$ measurement, the kink corresponds to the relative z' distance where the hydrogen on the tip apex can relax onto a lower potential energy surface. Chemically, CoH is transformed into CoH_2, a magnetically distinct complex with a different potential energy surface. DFT calculations show that the transition between the two distinct chemical configurations proceeds via a continuum of intermediate transition states. This intermediate regime is characterized by hydrogen on the tip sharing its bond with the tip apex and the CoH while simultaneously undergoing reorientation within the junction. In tackling this complexity, it is instructive to examine the diabatic potential energy surfaces in the limiting cases, that is, when CoH interacts with a hydrogen-functionalized tip and when CoH_2 interacts with a clean metallic tip. In Fig. 3D, we plot the dependence of the total energies of the two abovementioned configurations (red dash-dotted and blue dashed curves, respectively) on the

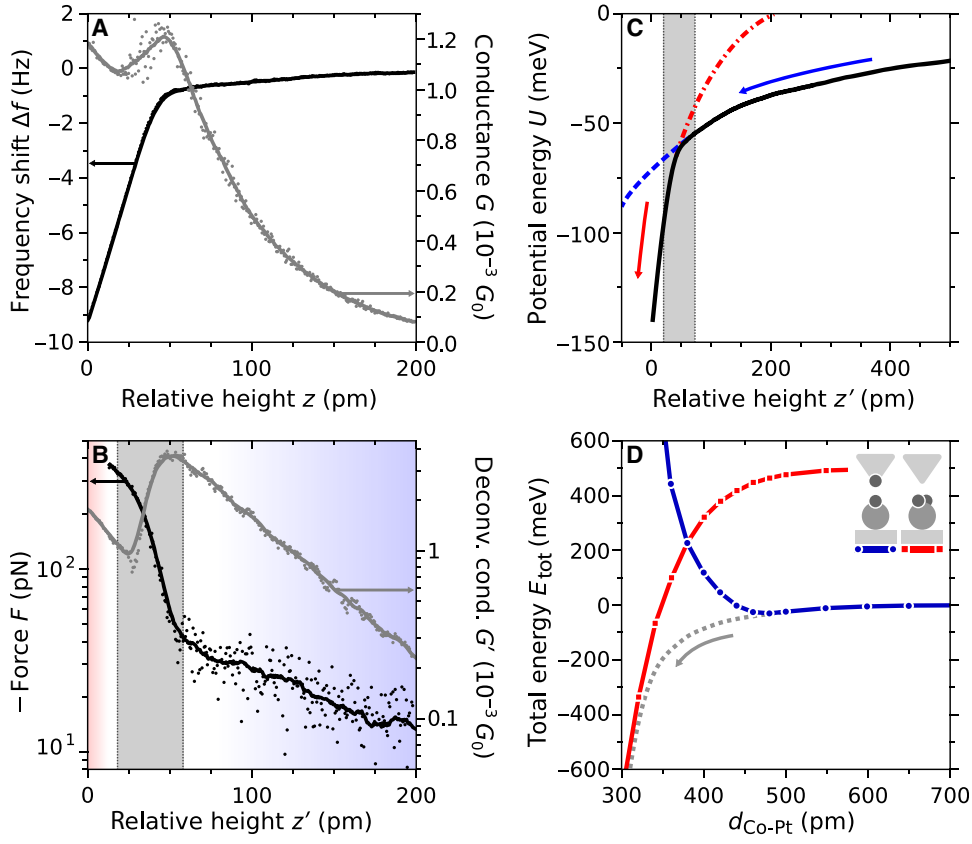

Fig. 3. Force measurements on a switching complex. (**A**) Simultaneous frequency shift–distance [$\Delta f(z)$ (black)] and conductance-distance [$G(z)$ (gray)] measurements at $V = -10$ mV on a CoH $S = 1$ complex with hydrogen-functionalized tip. The spin transition, occurring at a relative height z of 50 pm, is evident in both force and conductance channels. (**B**) Frequency shift was converted to short-range forces (black), and the conductance was deconvoluted to remove averaging over the oscillation amplitude (gray). On either side of the transition region, the deconvoluted conductance (Deconv. cond.) and force increase exponentially and can be described by the expressions $G(z') = G_0\exp(-2\kappa_G(z_0 + z'))$ and $F(z') = F_0\exp(-2\kappa_F(z_0 + z'))$, respectively. Inverse decay constants: κ_G, 13.0 ± 0.5 nm^{-1} ($0 < z' < 30$ pm) and 9.5 ± 0.1 nm^{-1} ($70 < z' < 200$ pm); κ_F, 10.0 ± 0.5 nm^{-1} ($0 < z' < 30$ pm) and 4.2 ± 0.3 nm^{-1} ($70 < z' < 200$ pm). (**C**) Interaction potential energy surface during the $S = 1$ to $S = {}^1/_2$ transition (black), determined by integrating the experimental $F(z')$ data. Dashed lines highlight the change in slope and indicate the point where a lower potential energy surface becomes accessible. Vertical dotted lines in (B) and (C) indicate the transition regime. For all curves, zero distance corresponds to the point of closest approach. (**D**) Simulated diabatic potential energy curves for a CoH/*h*-BN/Rh(111) complex approached by a hydrogen-functionalized Pt tip (blue dash-dotted curve) and a CoH_2 approached with a bare tip (red dash-dotted curve). The approximate adiabatic curve is shown as the gray dotted line. The reaction coordinate $d_{\mathrm{Co\text{-}Pt}}$ is the distance between the Co and the apex Pt atoms.

tip-sample distance d (see Materials and Methods and fig. S4), the chosen reaction coordinate for our system. The intersection of the two potential energy curves with varying junction width confirms that hydrogen transfer drives the spin transition and is consistent with experimental observations. As mentioned above, the system does not follow the diabatic curves; rather, it undergoes a barrierless transition along a reaction path difficult to precisely identify by ab initio methods because of the shallowness and unevenness of the hydrogen potential energy landscape in the junction. An approximate shape of this pathway is shown in Fig. 3D, with a gray dotted line linking the two asymptotic cases. The presence of a transition region (gray region in Fig. 3, B and C) further indicates that the spin switching is driven by the approaching hydrogen and that the residence time is shorter than the measurement time, leading to averaging and smearing-out when probed with the oscillating tip. Furthermore, the increased mechanical dissipation during the transition (~55 meV per cycle) (see fig. S5) is in good agreement with the potential energy difference across the transition region of the $U(z')$ measurement (~35 meV) and points to the existence of hysteresis on the time scale of the oscillation period of $(2f_0)^{-1} \sim 15$ µs.

DISCUSSION

We have reversibly switched the spin state of cobalt hydride complexes in a tunnel junction by using the hydrogen on the tip apex as a tunable ligand. During the total spin change, a transition region exists where the hydrogen can occupy two nearly equivalent sites separated only by a negligible barrier. As the junction conductance is altered, site equivalence is removed, and the tip displacement shifts the system to a preferred site. Beyond total spin, interactions with the tip determine how the cobalt spin couples with the host electron bath and whether a correlated Kondo state emerges. The relative stability of the double potential well and the possible occurrence of correlations are expected to be dependent on the materials used and the reactivity of the adsorbed molecule on the tip and the undercoordinated adatom. Reconstructing the 1D potential energy landscape shows that chemical transformation within the junction is responsible for the change of the total spin. Our measurements highlight how tip functionalization can influence the spin under investigation and suggests that they may be used to tailor molecular spins in ways difficult to achieve through traditional chemical synthesis.

MATERIALS AND METHODS

The clean Rh(111) surface was prepared by multiple cycles of argon ion sputtering and annealing to 1100 K in an ultrahigh vacuum chamber. During the final annealing cycle, borazine ($B_3N_3H_6$) gas was exposed to the hot sample at a pressure of 1.2×10^{-6} mbar for about ~2 min, resulting in a monoatomic layer of h-BN. Subsequently, the sample was cooled down (~20 K), and cobalt was deposited via an electron beam evaporator. Because hydrogen is the predominant component of the residual gas background, it is responsible for the formation of the cobalt hydride complexes. STM/AFM experiments were performed on a homebuilt instrument operating in ultrahigh vacuum at a base temperature of 1.1 K. All spectroscopic (dI/dV) measurements were obtained by adding a small sinusoidal voltage ($V_{mod} = 0.2$ mV, $f_{mod} = 600$ to 800 Hz) to the bias voltage V and using an external lock-in amplifier. We used $V = -10$ mV to adjust the conductance G before recording dI/dV curves by varying V at constant z, as well as to record $G(z)$ and $\Delta f(z)$ curves at constant V. Hydrogen pickup occurred fortuitously as the experiments went on, for example, during the approach of an initial CoH_x ($x = 1$ to 2) complex with a nonfunctionalized tip. Hydrogen-terminated tips were initially identified by features such as enhanced contrast in constant current imaging and then verified by the characteristic nonexponential behavior in $G(z)$ measurements (Fig. 2B, green).

The quartz tuning fork has a resonance frequency of $f_0 = 29{,}077$ Hz and a quality factor of approximately 10,000. Oscillation amplitudes of 100 pm were used. For the frequency shift curves, $\Delta f(z)$, the tip was positioned above the CoH complex with the oscillating tuning fork. The feedback loop was disabled, and the oscillating tip then approached 200 to 300 pm toward the sample and back. Immediately after completion, a retract curve was obtained by moving 2000 pm away from the surface (see fig. S3). When this sequence was completed, the tip was moved at constant height to the bare h-BN, and $\Delta f_{h\text{-BN}}$ was obtained. The frequency shift due to short-range forces was obtained by taking the difference $\Delta f = \Delta f_{CoH} - \Delta f_{h\text{-BN}}$. We distinguish between time-averaged signals at tip heights z and deconvoluted (instantaneous) signals at tip heights z'.

First-principles calculations were carried out in a manner consistent with the calculations used in our previous work (*5*). Briefly, a DFT approach, based on the projector augmented wave method (*27*) and a plane wave basis set (*28*), was used as implemented in the Vienna Ab initio Simulation Package (*29*). Exchange and correlation were treated with the gradient-corrected functional as formalized in PBE (Perdew, Burke, Ernzerhof) (*30*). On-site Coulomb interaction corrections were accounted for in the framework of the LSDA+U (local spin density approximation including Hubbard U) formalism, as introduced by Dudarev *et al.* (*31*). The considered geometry of the system was identical to the one introduced in the study by Jacobson *et al.* (*5*), that is, a Rh(111) surface was simulated by five Rh layers, on top of which an h-BN sheet was deposited (considered to be commensurate for computational feasibility reasons). A CoH complex was residing on top of an N atom of the h-BN sheet. The tip was simulated by a Pt pyramid of four atoms attached to an Rh surface. Before the tip approach simulation, the tip and the sample were allowed to relax. After placing the tip in the vicinity of the CoH_x complex, the CoH_x complex and the apex atom of the tip (as well as the attached hydrogen atom, where appropriate) were allowed to relax again, assuming an equilibrium static configuration. A full relaxation of the tip and the h-BN atoms around the CoH_x complex was tested and not found to introduce any change to the results above the calculation error level. In the experimentally relevant case of a CoH complex being approached with a singly hydrogenated tip, we are thus left with four atoms allowed to relax in three dimensions, amounting to a 12D configuration space. However, in effect, both the tip apex Pt and the Co atoms were found to experience only vertical relaxations, which, according to our tests, result in a minor quantitative change of the total energies and magnetic moments. This complies with our understanding of the mechanism of CoH_x complex spin switching, the latter being governed by the Co–H bonding, which, in turn, is altered through the rearrangement of the hydrogen atoms. To underline this fact, the calculation results presented in Fig. 3D and fig. S6 were obtained in a diabatic fashion, meaning that the initial relative orientation of the CoH_x and the $TipH_{2-x}$ atoms were kept frozen and that only the distance between the tip and the sample (characterized by the distance d between Co and apex Pt atoms) (see fig. S4) was varied. For hydrogen adsorption and transfer energies as well as the adiabatic transition calculation, the junction was allowed to relax.

SUPPLEMENTARY MATERIALS

Supplementary material for this article is available at http://advances.sciencemag.org/cgi/content/full/3/4/e1602060/DC1

fig. S1. Reversibility of the switching process.

fig. S2. Bias- and polarity-dependent $\Delta f(z)$ curves.
fig. S3. Long-range background subtraction.
fig. S4. Schematic drawing of the simulated junction geometry.
fig. S5. Measured dissipation across the spin transition.
fig. S6. Calculated magnetic moment as a function of Co-Pt separation.

REFERENCES AND NOTES

1. A. F. Otte, M. Ternes, K. von Bergmann, S. Loth, H. Brune, C. P. Lutz, C. F. Hirjibehedin, A. J. Heinrich, The role of magnetic anisotropy in the Kondo effect. *Nat. Phys.* **4**, 847–850 (2008).
2. S. Kahle, Z. Deng, N. Malinowski, C. Tonnoir, A. Forment-Aliaga, N. Thontasen, G. Rinke, D. Le, V. Turkowski, T. S. Rahman, S. Rauschenbach, M. Ternes, K. Kern, The quantum magnetism of individual manganese-12-acetate molecular magnets anchored at surfaces. *Nano Lett.* **12**, 518–521 (2012).
3. I. G. Rau, S. Baumann, S. Rusponi, F. Donati, S. Stepanow, L. Gragnaniello, J. Dreiser, C. Piamonteze, F. Nolting, S. Gangopadhyay, O. R. Albertini, R. M. Macfarlane, C. P. Lutz, B. A. Jones, P. Gambardella, A. J. Heinrich, H. Brune, Reaching the magnetic anisotropy limit of a 3d metal atom. *Science* **344**, 988–992 (2014).
4. J. C. Oberg, M. R. Calvo, F. Delgado, M. Moro-Lagares, D. Serrate, D. Jacob, J. Fernández-Rossier, C. F. Hirjibehedin, Control of single-spin magnetic anisotropy by exchange coupling. *Nat. Nanotechnol.* **9**, 64–68 (2014).
5. P. Jacobson, T. Herden, M. Muenks, G. Laskin, O. Brovko, V. Stepanyuk, M. Ternes, K. Kern, Quantum engineering of spin and anisotropy in magnetic molecular junctions. *Nat. Commun.* **6**, 8536 (2015).
6. B. W. Heinrich, L. Braun, J. I. Pascual, K. J. Franke, Tuning the magnetic anisotropy of single molecules. *Nano Lett.* **15**, 4024–4028 (2015).
7. J. J. Parks, A. R. Champagne, T. A. Costi, W. W. Shum, A. N. Pasupathy, E. Neuscamman, S. Flores-Torres, P. S. Cornaglia, A. A. Aligia, C. A. Balseiro, G. K.-L. Chan, H. D. Abruña, D. C. Ralph, Mechanical control of spin states in spin-1 molecules and the underscreened Kondo effect. *Science* **328**, 1370–1373 (2010).
8. D. M. Eigler, E. K. Schweizer, Positioning single atoms with a scanning tunnelling microscope. *Nature* **344**, 524–526 (1990).
9. D. M. Eigler, C. P. Lutz, W. E. Rudge, An atomic switch realized with the scanning tunnelling microscope. *Nature* **352**, 600–603 (1991).
10. O. Custance, R. Perez, S. Morita, Atomic force microscopy as a tool for atom manipulation. *Nat. Nanotechnol.* **4**, 803–810 (2009).
11. J. Bork, Y.-h. Zhang, L. Diekhöner, L. Borda, P. Simon, J. Kroha, P. Wahl, K. Kern, A tunable two-impurity Kondo system in an atomic point contact. *Nat. Phys.* **7**, 901–906 (2011).
12. D.-J. Choi, M. V. Rastei, P. Simon, L. Limot, Conductance-driven change of the Kondo effect in a single cobalt atom. *Phys. Rev. Lett.* **108**, 266803 (2012).
13. M. Muenks, P. Jacobson, M. Ternes, K. Kern, Correlation-driven transport asymmetries through coupled spins in a tunnel junction. *Nat. Commun.* **8**, 14119 (2017).
14. C. Wagner, R. Temirov, Tunnelling junctions with additional degrees of freedom: An extended toolbox of scanning probe microscopy. *Prog. Surf. Sci.* **90**, 194–222 (2015).
15. L. Bartels, G. Meyer, K.-H. Rieder, Controlled vertical manipulation of single CO molecules with the scanning tunneling microscope: A route to chemical contrast. *Appl. Phys. Lett.* **71**, 213–215 (1997).
16. A. J. Weymouth, T. Hofmann, F. J. Giessibl, Quantifying molecular stiffness and interaction with lateral force microscopy. *Science* **343**, 1120–1122 (2014).
17. G. Kichin, C. Weiss, C. Wagner, F. S. Tautz, R. Temirov, Single molecule and single atom sensors for atomic resolution imaging of chemically complex surfaces. *J. Am. Chem. Soc.* **133**, 16847–16851 (2011).
18. C. Weiss, C. Wagner, C. Kleimann, M. Rohlfing, F. S. Tautz, R. Temirov, Imaging Pauli repulsion in scanning tunneling microscopy. *Phys. Rev. Lett.* **105**, 086103 (2010).
19. H. Wende, M. Bernien, J. Luo, C. Sorg, N. Ponpandian, J. Kurde, J. Miguel, M. Piantek, X. Xu, P. Eckhold, W. Kuch, K. Baberschke, P. M. Panchmatia, B. Sanyal, P. M. Oppeneer, O. Eriksson, Substrate-induced magnetic ordering and switching of iron porphyrin molecules. *Nat. Mater.* **6**, 516–520 (2007).
20. C. Wäckerlin, K. Tarafder, D. Siewert, J. Girovsky, T. Hählen, C. Iacovita, A. Kleibert, F. Nolting, T. A. Jung, P. M. Oppeneerb, N. Ballav, On-surface coordination chemistry of planar molecular spin systems: Novel magnetochemical effects induced by axial ligands. *Chem. Sci.* **3**, 3154–3160 (2012).
21. R. Temirov, S. Soubatch, O. Neucheva, A. C. Lassise, F. S. Tautz, A novel method achieving ultra-high geometrical resolution in scanning tunnelling microscopy. *New J. Phys.* **10**, 053012 (2008).
22. M. Pivetta, M. Ternes, F. Patthey, W.-D. Schneider, Diatomic molecular switches to enable the observation of very-low-energy vibrations. *Phys. Rev. Lett.* **99**, 126104 (2007).
23. T. Esat, T. Deilmann, B. Lechtenberg, C. Wagner, P. Krüger, R. Temirov, F. B. Anders, M. Rohlfing, F. S. Tautz, Transfering spin into an extended π orbital of a large molecule. *Phys. Rev. B* **91**, 144415 (2015).
24. J. E. Sader, S. P. Jarvis, Accurate formulas for interaction force and energy in frequency modulation force spectroscopy. *Appl. Phys. Lett.* **84**, 1801 (2004).
25. J. E. Sader, Y. Sugimoto, Accurate formula for conversion of tunneling current in dynamic atomic force spectroscopy. *Appl. Phys. Lett.* **97**, 043502 (2010).
26. P. Hapala, G. Kichin, C. Wagner, F. S. Tautz, R. Temirov, P. Jelínek, Mechanism of high-resolution STM/AFM imaging with functionalized tips. *Phys. Rev. B* **90**, 085421 (2014).
27. P. E. Blöchl, Projector augmented-wave method. *Phys. Rev. B* **50**, 17953–17979 (1994).
28. G. Kresse, J. Furthmüller, Efficient iterative schemes for ab initio total-energy calculations using a plane-wave basis set. *Phys. Rev. B* **54**, 11169–11186 (1996).
29. G. Kresse, J. Hafner, Ab initio molecular dynamics for liquid metals. *Phys. Rev. B* **47**, 558–561 (1993).
30. J. P. Perdew, K. Burke, M. Ernzerhof, Generalized gradient approximation made simple. *Phys. Rev. Lett.* **77**, 3865–3868 (1996).
31. S. L. Dudarev, G. A. Botton, S. Y. Savrasov, C. J. Humphreys, A. P. Sutton, Electron-energy-loss spectra and the structural stability of nickel oxide: An LSDA+U study. *Phys. Rev. B* **57**, 1505–1509 (1998).

Acknowledgments: We thank U. Schlickum for fruitful discussions, F. Giessibl for providing quartz tuning forks, and M. Mausser for focused ion beam cutting of the Pt tips. **Funding:** P.J. acknowledges support from the Alexander von Humboldt Foundation. M.M. and M.T. acknowledge support from the Sonderforschungsbereich 767 (SFB 767). O.B. and V.S. acknowledge support from the SFB 762. O.B. acknowledges support from the European Research Council grant no. 320796, MODPHYSFRICT. **Author contributions:** M.T. and K.K. conceived the project. P.J., M.M., and G.L. performed the measurements. P.J., M.M., and M.T. analyzed the data. O.B. and V.S. performed the DFT calculations. P.J. drafted the manuscript, and all authors contributed to the manuscript. **Competing interests:** The authors declare that they have no competing interests. **Data and materials availability:** All data needed to evaluate the conclusions in the paper are present in the paper and/or the Supplementary Materials. Additional data related to this paper may be requested from the authors.

Submitted 29 August 2016
Accepted 19 February 2017
Published 14 April 2017
10.1126/sciadv.1602060

Citation: P. Jacobson, M. Muenks, G. Laskin, O. Brovko, V. Stepanyuk, M. Ternes, K. Kern, Potential energy–driven spin manipulation via a controllable hydrogen ligand. *Sci. Adv.* **3**, e1602060 (2017).

Science Advances

Potential energy–driven spin manipulation via a controllable hydrogen ligand

Peter Jacobson, Matthias Muenks, Gennadii Laskin, Oleg Brovko, Valeri Stepanyuk, Markus Ternes and Klaus Kern

Sci Adv **3** (4), e1602060.
DOI: 10.1126/sciadv.1602060